THE FLEXIBILITY OF FUNCTIONALLY GRADED MATERIAL PLATES SUBJECTED TO UNIFORM LOADS

Yen-Ling Chung and Wei-Ting Chen

THE FLEXIBILITY OF FUNCTIONALLY GRADED MATERIAL PLATES SUBJECTED TO UNIFORM LOADS

YEN-LING CHUNG AND WEI-TING CHEN

We analyze functionally graded material (FGM) plates with two opposite edges simply supported and the other two edges free subjected to a uniform load. Even though an FGM plate is a kind of composite material, if the Young's modulus of the FGM plates varies along the thickness direction and the Poisson's ratio is constant in the whole FGM plate, the bending and in-plane problems in FGM plates under transverse load only are uncoupled. Therefore, the analytical solution to the bending problem of FGM plates is obtained in this study by Fourier series expansions, which agrees very well with a finite element calculation. Results show that the maximum tensile stresses are located at the bottom of the FGM plates. However, the maximum compressive stresses move to the inside of the FGM plates. The coefficients A_{11}, B_{11}, C_{11} defined in this paper relate to the area and to the first and the second moments of the area under the $E(z)$ curve from $z = -h/2$ to $z = h/2$. The parameter Q_{11}, representing the location of the centroid of the area under the $E(z)$ curve, is related to the location of the neutral surfaces, and S_{11} represents the bending stiffness of the FGM plates.

1. Introduction

Functionally graded materials (FGMs), a type of composite material produced by continuously varying the volume fractions in the thickness direction to obtain a predetermined profile, have received much attention recently because of the advantages of decreasing the mismatch in material properties and reducing residual and thermal stresses [Chung and Chi 2001; Lee and Erdogan 1994]. Many researchers have been working toward an understanding of the material constituent [Chi and Chung 2002; Bao and Wang 1995; Suresh and Mortensen 1998], fracture mechanics [Chi and Chung 2003; Jin and Noda 1994; Jin and Batra 1996; Delale and Erdogan 1983; Gu and Asaro 1997; Cai and Bao 1998; Jin and Paulino 2001; Erdogan and Wu 1996; Erdogan and Chen 1998], and processing of FGMs [Kwon and Crimp 1997; Kesler et al. 1997].

FGMs may be applied to plate structures in aircraft, space vehicles, reactor vessels, and other engineering applications as a thermal barrier. Studies of thermoelastic deformations of FGM plates can be found in many references in the literature. Obata and Noda [1996] theoretically analyzed and numerically calculated the steady thermal stresses in an FGM plate composed of PSZ and Ti-6Al-4V, and determined the optimal FGM plates. Praveen and Reddy [1998] investigated nonlinear transient thermoelastic responses of functionally graded ceramic-metal plates by using a plate finite element that accounts for the transverse shear strains, rotary inertia and moderately large rotations in the Von Karman sense. An exact solution was obtained in [Vel and Batra 2002] for three-dimensional deformations of a simply supported FGM thick rectangular plate subjected to mechanical and thermal loads on its top and/or bottom surfaces.

Keywords: FGM plate, Fourier series expansion, finite element analysis.

The exact solutions for mechanical and thermal loads are used to assess the accuracy of classical plate theory, first-order shear deformation theory, and a third-order shear deformation theory. Transient thermal stresses in FGM plates with a simple power-law distribution were investigated in [Vel and Batra 2003].

Buckling behavior plays an important role in plate structures. Elastic bifurcation buckling of FGM plates under in-plane compressive loading was studied in [Feldman and Aboudi 1997], based on a combination of micromechanical and structural approaches. Ma and Wang [2004] investigated the axisymmetric bending and buckling solutions for an FGM circular plate based on third-order plate theory and classical plate theory. The results showed that the first-order shear deformation plate theory is enough to consider the effect of shear deformation on the axisymmetric bending and buckling of FGM plates. The problems of thermal buckling in the axial direction of cylindrical shells made of FGMs varying as a power form were discussed in [Wu et al. 2005]. Moreover, the dynamic stability of conical FGM shells subjected to a periodic impulsive pressure was studied in [Sofiyev 2004] by applying Galerkin's method.

Understanding of the mechanical behavior of an FGM plate becomes very important in assessing the safety of the plate structure. Woo and Meguid [2001] applied Karman theory for large deformations to obtain the analytical solution for plates and shells under transverse mechanical loads and a temperature field. He et al. [2001] studied the vibration control of the FGM plates with integrated piezoelectric sensors and actuators by a finite element formulation based on the classical laminated plate theory. Chi and Chung [2006a; 2006b] analyzed the mechanical behaviors of a simply supported rectangular FGM plate with sigmoid functions of the volume fraction of the constituents by the Fourier series expansion. The collocation multiquadric radial basis is used in [Ferreira et al. 2005] to analyze static deformations of simply supported FGMs modeled by a third-order shear deformation theory and a meshless method.

The closed-form solution to the problems of FGM plates subjected to transverse loads with two opposite edges simply supported and the other two edges free is not found in the literature. Therefore, this study will focus on the simple but important problems of FGM plates with two opposite edges simply supported and the other two edges free. The material properties of the FGM plates considered here are assumed to change continuously throughout the thickness of the plate, according to the volume fraction of the constituent material based on the power-law and sigmoid functions. The analytical solution is obtained by the Fourier series expansion and compared with the finite element calculation.

2. Governing equations

Consider a linearly elastic, moderately thick, rectangular FGM plate subjected to a transverse load. Assume the plate has a uniform thickness h in the range $1/20 \sim 1/100$ of its span. The deformations and the stresses of the FGM plate are derived under the following assumptions:

1. Line elements perpendicular to the middle surface of the plate before deformation remain normal and unstretched after deformation.

2. The deflection of the FGM plate is small in comparison with its thickness h, so the linear strain-displacement relations are valid.

3. The normal stress in the thickness direction can be neglected because of the thickness assumption.

4. For the nonhomogeneous elastic FGM plate, the Young's modulus and Poisson's ratio of the FGM plate are functions of the spatial coordinate z.

2.1. Stress field of FGM plates. According to assumption 1, the transverse strain components ε_{zz}, γ_{xz}, and γ_{yz} are negligibly small. Under the assumption of small deformation, the strain field of the FGM plate is

$$\varepsilon_x = \frac{\partial u}{\partial x} = \varepsilon_{x_0} - z\frac{\partial^2 w(x,y)}{\partial x^2}, \tag{1a}$$

$$\varepsilon_y = \frac{\partial v}{\partial y} = \varepsilon_{y_0} - z\frac{\partial^2 w(x,y)}{\partial y^2}, \tag{1b}$$

$$\gamma_{xy} = \frac{\partial u}{\partial y} + \frac{\partial v}{\partial x} = \gamma_{xy_0} - 2z\frac{\partial^2 w(x,y)}{\partial x \partial y}, \tag{1c}$$

$$\varepsilon_z = \gamma_{xz} = \gamma_{yz} = 0, \tag{1d}$$

where

$$\varepsilon_{x_0} = \frac{\partial u_0(x,y)}{\partial x} \qquad \varepsilon_{y_0} = \frac{\partial v_0(x,y)}{\partial y} \qquad \gamma_{xy_0} = \frac{\partial u_0}{\partial y} + \frac{\partial v_0}{\partial x}$$

are strains at the middle surface. The quantities $u_0(x,y)$, $v_0(x,y)$, $w_0(x,y)$ are the displacements at the middle surface. It is known that neglecting the transverse shear deformations may lead to significant errors when applied to moderately thick plates with thickness larger than 0.1 of span [Tauchert 1986]. However, Shames and Dym [1985] indicated that for a plate with a thickness less than 0.1 of its span, the classical theory of plates is expected to give good results. In this paper, the thickness of the moderately thick FGM plate is assumed to be in the range $1/20 \sim 1/100$ of its span, therefore the transverse shear deformations are negligible.

Based on assumptions 3 and 4, the stress-strain relation of an FGM plate for plane stress condition is

$$\sigma_x = \frac{E(z)}{1-v(z)^2}\left(\varepsilon_{x_0} + v(z)\varepsilon_{y_0} - z\left(\frac{\partial^2 w}{\partial x^2} + v(z)\frac{\partial^2 w}{\partial y^2}\right)\right), \tag{2a}$$

$$\sigma_y = \frac{E(z)}{1-v(z)^2}\left(\varepsilon_{y_0} + v(z)\varepsilon_{x_0} - z\left(\frac{\partial^2 w}{\partial y^2} + v(z)\frac{\partial^2 w}{\partial x^2}\right)\right), \tag{2b}$$

$$\tau_{xy} = \frac{E(z)}{1-v(z)^2}\left(\frac{1-v(z)}{2}\right)\left(\gamma_{xy_0} - 2z\frac{\partial^2 w}{\partial x \partial y}\right). \tag{2c}$$

2.2. Axial forces, shear forces, and bending moments of FGM plates. The stress resultants per unit length of the middle surface are defined by integrating stresses along the thickness. Thus the in-plane axial forces N_x, N_y, and N_{xy}, and the bending moments per unit length of the middle surface, M_x, M_y, and M_{xy} are defined as follows, with $\alpha = x, y$:

$$N_\alpha = \int_{-h/2}^{h/2} \sigma_\alpha \, dz, \qquad N_{xy} = \int_{-h/2}^{h/2} \tau_{xy} \, dz, \qquad M_\alpha = \int_{-h/2}^{h/2} z\sigma_\alpha \, dz, \qquad M_{xy} = \int_{-h/2}^{h/2} z\tau_{xy} \, dz.$$

Substituting the relations (2) into these defining equations, we obtain the in-plane axial forces and the bending moments in terms of the middle-surface strains and deflection:

$$
\begin{Bmatrix} N_x \\ N_y \\ N_{xy} \end{Bmatrix} = \begin{bmatrix} A_{11} & A_{12} & 0 \\ A_{12} & A_{11} & 0 \\ 0 & 0 & A_{66} \end{bmatrix} \begin{Bmatrix} \varepsilon_{x0} \\ \varepsilon_{y0} \\ \gamma_{xy0} \end{Bmatrix} + \begin{bmatrix} B_{11} & B_{12} & 0 \\ B_{12} & B_{11} & 0 \\ 0 & 0 & B_{66} \end{bmatrix} \begin{Bmatrix} -\dfrac{\partial^2 w}{\partial x^2} \\ -\dfrac{\partial^2 w}{\partial y^2} \\ -2\dfrac{\partial^2 w}{\partial x \partial y} \end{Bmatrix}, \tag{3}
$$

$$
\begin{Bmatrix} M_x \\ M_y \\ M_{xy} \end{Bmatrix} = \begin{bmatrix} B_{11} & B_{12} & 0 \\ B_{12} & B_{11} & 0 \\ 0 & 0 & B_{66} \end{bmatrix} \begin{Bmatrix} \varepsilon_{x0} \\ \varepsilon_{y0} \\ \gamma_{xy0} \end{Bmatrix} + \begin{bmatrix} C_{11} & C_{12} & 0 \\ C_{12} & C_{11} & 0 \\ 0 & 0 & C_{66} \end{bmatrix} \begin{Bmatrix} -\dfrac{\partial^2 w}{\partial x^2} \\ -\dfrac{\partial^2 w}{\partial y^2} \\ -2\dfrac{\partial^2 w}{\partial x \partial y} \end{Bmatrix}, \tag{4}
$$

where the coefficients of A_{ij}, B_{ij} and C_{ij} are the integration of the material properties of the FGM plate

$$
(A_{11}, B_{11}, C_{11}) = \int_{-h/2}^{h/2} \frac{1}{1 - v(z)^2} \big(E(z), zE(z), z^2 E(z)\big)\, dz, \tag{5a}
$$

$$
(A_{12}, B_{12}, C_{12}) = \int_{-h/2}^{h/2} \frac{v}{1 - v(z)^2} \big(E(z), zE(z), z^2 E(z)\big)\, dz, \tag{5b}
$$

$$
(A_{66}, B_{66}, C_{66}) = \int_{-h/2}^{h/2} \frac{1}{2(1 + v(z))} \big(E(z), zE(z), z^2 E(z)\big)\, dz. \tag{5c}
$$

2.3. Equilibrium and compatibility equations for FGM plates. Assume that the FGM plate is subjected to the distributed loads q_x, q_y and q_z along the x, y and z directions. Then the equilibrium equations of the FGM plate are (see [Chi and Chung 2003])

$$
\frac{\partial N_x}{\partial x} + \frac{\partial N_{yx}}{\partial y} + q_x = 0 \tag{6}
$$

$$
\frac{\partial N_{yx}}{\partial x} + \frac{\partial N_y}{\partial y} + q_y = 0 \tag{7}
$$

$$
\frac{\partial^2 M_x}{\partial x^2} + 2\frac{\partial^2 M_{xy}}{\partial x \partial y} + \frac{\partial^2 M_y}{\partial y^2} = -q_z(x, y). \tag{8}
$$

If the FGM plate is only subjected to the transverse load q_z, that is, if $q_x = q_y = 0$, the in-plane Equations (6) and (7) can be solved in term of a stress function $\phi(x, y)$ defined by

$$
N_x = \frac{\partial^2 \phi}{\partial y^2}; \qquad N_y = \frac{\partial^2 \phi}{\partial x^2}; \qquad N_{xy} = -\frac{\partial^2 \phi}{\partial x \partial y}. \tag{9}
$$

Using Equations (3) and (9), the strains at the middle surface are then expressed in terms of the stress function $\phi(x, y)$ and the deflection w as

$$
\left\{
\begin{array}{c}
\varepsilon_{x_0} \\
\varepsilon_{y_0} \\
\gamma_{xy_0}
\end{array}
\right\}
=
\begin{bmatrix}
P_{11} & P_{12} & 0 \\
P_{12} & P_{11} & 0 \\
0 & 0 & P_{66}
\end{bmatrix}
\left\{
\begin{array}{c}
\dfrac{\partial^2 \phi}{\partial y^2} \\[2mm]
\dfrac{\partial^2 \phi}{\partial x^2} \\[2mm]
\dfrac{\partial^2 \phi}{\partial x \partial y}
\end{array}
\right\}
+
\begin{bmatrix}
Q_{11} & Q_{12} & 0 \\
Q_{12} & Q_{11} & 0 \\
0 & 0 & Q_{66}
\end{bmatrix}
\left\{
\begin{array}{c}
-\dfrac{\partial^2 w}{\partial x^2} \\[2mm]
-\dfrac{\partial^2 w}{\partial y^2} \\[2mm]
-2\dfrac{\partial^2 w}{\partial x \partial y}
\end{array}
\right\}.
\tag{10}
$$

Consequently, the bending moments rearranged by substituting (10) into (4) are

$$
\left\{
\begin{array}{c}
M_x \\
M_y \\
M_{xy}
\end{array}
\right\}
=
\begin{bmatrix}
-Q_{11} & -Q_{12} & 0 \\
-Q_{12} & -Q_{11} & 0 \\
0 & 0 & -Q_{66}
\end{bmatrix}
\left\{
\begin{array}{c}
\dfrac{\partial^2 \phi}{\partial y^2} \\[2mm]
\dfrac{\partial^2 \phi}{\partial x^2} \\[2mm]
\dfrac{\partial^2 \phi}{\partial x \partial y}
\end{array}
\right\}
+
\begin{bmatrix}
S_{11} & S_{12} & 0 \\
S_{12} & S_{11} & 0 \\
0 & 0 & S_{66}
\end{bmatrix}
\left\{
\begin{array}{c}
-\dfrac{\partial^2 w}{\partial x^2} \\[2mm]
-\dfrac{\partial^2 w}{\partial y^2} \\[2mm]
-2\dfrac{\partial^2 w}{\partial x \partial y}
\end{array}
\right\},
\tag{11}
$$

where

$$
\begin{aligned}
P_{11} &= A_{11}/\Delta, & Q_{11} &= (A_{12}B_{12} - A_{11}B_{11})/\Delta, & S_{11} &= B_{11}Q_{11} + B_{12}Q_{12} + C_{11}, \\
P_{12} &= -A_{12}/\Delta, & Q_{12} &= (A_{12}B_{11} - A_{11}B_{12})/\Delta, & S_{12} &= B_{11}Q_{12} + B_{12}Q_{11} + C_{12}, \\
P_{66} &= -1/A_{66}, & Q_{66} &= -B_{66}/A_{66}, & S_{66} &= C_{66} + B_{66}Q_{66},
\end{aligned}
\tag{12}
$$

and

$$
\Delta = A_{11}^2 - A_{12}^2.
$$

Consequently, we substitute (11) into (8) and the equilibrium equation becomes

$$
Q_{12}\frac{\partial^4 \phi}{\partial x^4} + 2(Q_{11} - Q_{66})\frac{\partial^4 \phi}{\partial x^2 \partial y^2} + Q_{12}\frac{\partial^4 \phi}{\partial y^4} + S_{11}\frac{\partial^4 w}{\partial x^4} + 2(S_{12} + 2S_{66})\frac{\partial^4 w}{\partial x^2 \partial y^2} + S_{11}\frac{\partial^4 w}{\partial y^4} = q_z(x, y).
\tag{13}
$$

In a similar manner, the compatibility equation for a plane problem expressed in terms of stress function $\phi(x, y)$ and the deflection w are derived as

$$
P_{11}\frac{\partial^4 \phi}{\partial x^4} + (2P_{12} - P_{66})\frac{\partial^4 \phi}{\partial x^2 \partial y^2} + P_{11}\frac{\partial^4 \phi}{\partial y^4} - Q_{12}\frac{\partial^4 w}{\partial x^4} - 2(Q_{11} - Q_{66})\frac{\partial^4 w}{\partial x^2 \partial y^2} - Q_{12}\frac{\partial^4 w}{\partial y^4} = 0.
\tag{14}
$$

Equations (13) and (14) provide the simultaneous equations to solve the stress function $\phi(x, y)$ and the deflection w. They are particular cases of the nonlinear equations presented in [Woo and Meguid 2001]. Similar formulae for the equilibrium and compatibility equations in (13) and (14) can also be found in [Nowinski and Turski 1953] and [Sokolowski 1958].

If both the Young's modulus and Poisson's ratio are considered for calculating the coefficient, the integration will turn out to be very complex. Chi and Chung [2003] showed that the influence of Poisson's ratio on the mechanics of FGM plates is much less than that of the Young's modulus. Therefore, the

solutions for the material with Poisson's ratio assumed to be constant and Young's modulus varying in the thickness direction are derived in Section 3.

For material with $\nu =$ constant and $E = E(z)$, it can be found that

$$
\begin{aligned}
(A_{12}, B_{12}, C_{12}) &= \nu(A_{11}, B_{11}, C_{11}), \\
(A_{66}, B_{66}, C_{66}) &= \frac{1-\nu}{2}(A_{11}, B_{11}, C_{11}), \\
(P_{12}, Q_{12}, S_{12}) &= \nu(-P_{11}, 0, S_{11}), \\
(P_{66}, Q_{66}, S_{66}) &= \left(-2(1+\nu)P_{11}, Q_{11}, \frac{1-\nu}{2}S_{11}\right),
\end{aligned}
\tag{15}
$$

where

$$
P_{11} = \frac{1}{(1-\nu^2)A_{11}}, \qquad Q_{11} = -\frac{B_{11}}{A_{11}}, \qquad \text{and} \qquad S_{11} = B_{11}Q_{11} + C_{11}.
$$

Consequently, the equilibrium and compatibility equations are simplified as

$$
S_{11}\nabla^4 w = q(x, y), \tag{16}
$$

$$
\nabla^4 \phi = 0. \tag{17}
$$

It can be seen that for the FGM plate with constant Poisson's ratio, the governing equations of the bending problem expressed in Equation (16) and the in-plane problem in Equation (17) are uncoupled.

3. Solution to FGM plates with two opposite edges simply supported and two other edges free

Consider an FGM plate with length a, width b, and uniform thickness h subjected to the lateral load $q_z(x, y)$. The coordinates x and y define the plane of the plate, whereas the z-axis originating at the middle surface of the plate is in the thickness direction. The Poisson's ratio of the FGM plate is assumed to be constant and the Young's modulus varies functionally in the thickness direction. Further assume that two opposite edges of the FGM plate are simply supported and the other edges are free, as shown in Figure 1.

The deflection w must satisfy the boundary conditions of $w = 0$ and $w'' = 0$ at $x = 0$ and $x = a$. Therefore the deflection of the FGM plate can be assumed as

$$
w(x, y) = \sum_{m=1}^{\infty} w_m(y) \sin \frac{m\pi x}{a}. \tag{18}
$$

Consequently the distributed loading $q_z(x, y)$ can be expanded by Fourier series

$$
q_z(x, y) = \sum_{m=1}^{\infty} q_m(y) \sin kx,
$$

where $q_m(y) = \int q_z(x, y) \sin kx \, dx$ and $k = m\pi/a$. For the special case when the FGM plate is under a uniform load with magnitude $q_z(x, y) = q_0$, the quantity $q_m(y) = 4q_0/(m\pi)$ where m is an odd number.
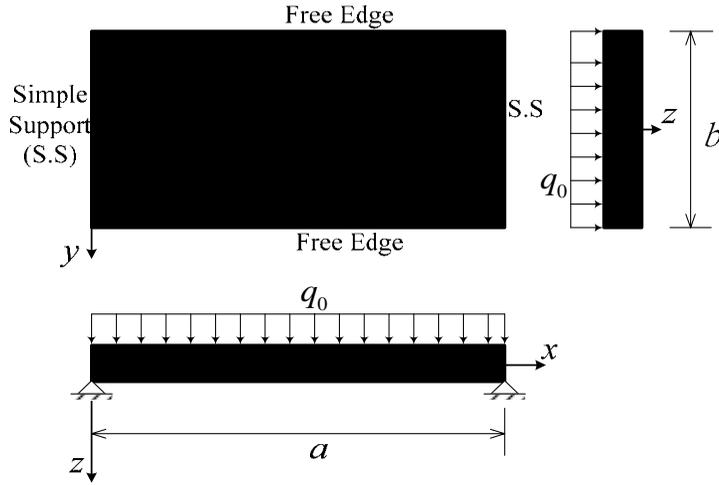
Figure 1. The configuration of an FGM plate.

To satisfy the governing equation of $\nabla^4 \phi = 0$, the stress function is also assumed as

$$\phi(x, y) = \sum_{m=1}^{\infty} \phi_m(y) \sin \frac{m\pi x}{a}. \tag{19}$$

Substituting (18) and (19) into (16) and (17), we rewrite the governing equations as

$$k^4 w_m(y) - 2k^2 w_m''(y) + w'''_m(y) = \frac{q_m(y)}{S_{11}}, \tag{20}$$

$$k^4 \phi_m(y) - 2k^2 \phi_m''(y) + \phi'''_m(y) = 0. \tag{21}$$

The solution of (20) consists of a homogeneous part $w_{mh}(y)$, and a particular part $w_{mp}(y)$. The particular part cannot be determined until $q_m(y)$ is specified. However, the homogeneous part can be easily determined as

$$w_{mh}(y) = A_{1m} \cosh ky + A_{2m} ky \sinh ky + A_{3m} \sinh ky + A_{4m} ky \cosh ky. \tag{22}$$

Similarly, $\phi_m(y)$ is obtained in the form

$$\phi_m(y) = B_{1m} \cosh ky + B_{2m} ky \sinh ky + B_{3m} \sinh ky + B_{4m} ky \cosh ky. \tag{23}$$

Because of symmetry with respect to the y-axis,

$$A_{3m} = A_{4m} = B_{3m} = B_{4m} = 0.$$

The unknown constants A_{im} and B_{im} can be determined from the boundary conditions on the free edges ($y = \pm b/2$) as

$$\begin{cases} M_y = 0, \\ V_y + \dfrac{\partial M_{xy}}{\partial y} = 0, \end{cases} \quad \text{and} \quad \begin{cases} N_y = 0, \\ N_{xy} = 0. \end{cases}$$

The conditions $N_y(y = \pm b/2) = 0$ and $N_{xy}(y = \pm b/2) = 0$ give $B_{1m} = B_{2m} = 0$. Consequently, the stress function $\phi(x, y) = 0$. The boundary conditions $M_y = 0$ and $V_y + \partial M_{xy}/\partial y = 0$ at $y = \pm b/2$ yield

$$A_{1m} = \frac{\nu w_{mp}(y)\left(\frac{1+\nu}{1-\nu}\sinh\frac{kb}{2} - \frac{kb}{2}\cosh\frac{kb}{2}\right)}{\frac{3+\nu}{2}\sinh kb - (1-\nu)\frac{kb}{2}}, \qquad A_{2m} = \frac{\nu w_{mp}(y)\sinh\frac{kb}{2}}{\frac{3+\nu}{2}\sinh kb - (1-\nu)\frac{kb}{2}}. \tag{24}$$

With the aid of $\phi(x, y) = 0$, the complete solution of the FGM plate with two opposite edges simply supported and two other edges free is

$$w(x, y) = \sum_m \left(A_{1m}\cosh ky + A_{2m}ky\sinh ky + w_{mp}(y)\right)\sin kx, \tag{25a}$$

$$N_x = N_y = N_{xy} = 0, \tag{25b}$$

$$\begin{Bmatrix} M_x \\ M_y \\ M_{xy} \end{Bmatrix} = S_{11}\begin{bmatrix} 1 & \nu & 0 \\ \nu & 1 & 0 \\ 0 & 0 & (1-\nu)/2 \end{bmatrix}\begin{Bmatrix} \kappa_x \\ \kappa_y \\ \kappa_{xy} \end{Bmatrix}, \tag{25c}$$

$$\begin{Bmatrix} \varepsilon_{x0} \\ \varepsilon_{y0} \\ \gamma_{xy0} \end{Bmatrix} = Q_{11}\begin{Bmatrix} \kappa_x \\ \kappa_y \\ \kappa_{xy} \end{Bmatrix}, \tag{25d}$$

$$\begin{Bmatrix} \varepsilon_x \\ \varepsilon_y \\ \gamma_{xy} \end{Bmatrix} = (Q_{11} + z)\begin{Bmatrix} \kappa_x \\ \kappa_y \\ \kappa_{xy} \end{Bmatrix}, \tag{25e}$$

$$\begin{Bmatrix} \sigma_x \\ \sigma_y \\ \tau_{xy} \end{Bmatrix} = \left(\frac{E(z)}{1-\nu^2}\right)\left(\frac{Q_{11} + z}{S_{11}}\right)\begin{Bmatrix} M_x \\ M_y \\ M_{xy} \end{Bmatrix}, \tag{25f}$$

where $\kappa_x = -\dfrac{\partial^2 w}{\partial x^2}$, $\kappa_y = -\dfrac{\partial^2 w}{\partial y^2}$, $\kappa_{xy} = -2\dfrac{\partial^2 w}{\partial x \partial y}$, and

$$\frac{\partial^2 w}{\partial x^2} = -\sum_m k^2\left(A_{1m}\cosh ky + A_{2m}ky\sinh ky + w_{mp}(y)\right)\sin kx,$$

$$\frac{\partial^2 w}{\partial y^2} = \sum_m k^2\left(A_{1m}\cosh ky + A_{2m}(2\cosh ky + ky\sinh ky) + w''_{mp}(y)\right)\sin kx,$$

$$\frac{\partial^2 w}{\partial x \partial y} = \sum_m k^2\left(A_{1m}\sinh ky + A_{2m}(\sinh ky + ky\cosh ky) + w'_{mp}(y)\right)\cos kx,$$

for an FGM plate under a uniform load with magnitude $q_z(x, y) = q_0$, the particular solution w_{mp} equals $4q_0/(ak^5 S_{11})$.

4. Material gradient and the physical meaning of the coefficients

For the FGM plate in Figure 1, Poisson's ratio is assumed to be constant. The Young's moduli on the upper and lower surfaces of the FGM plate differ and are preassigned according to the performance demands, but the Young's modulus inside FGM plates varies continuously in the thickness direction with power-law functions (P-FGM) or sigmoid functions (S-FGM).

4.1. *Material properties and parameters of P-FGM plates.* The volume fraction of the P-FGM is assumed to obey a power-law function

$$g(z) = \left(\frac{z + h/2}{h}\right)^p, \tag{26}$$

where p is the material parameter and h is the thickness of the plate. Once the local volume fraction $g(z)$ has been defined, the material properties of a P-FGM can be determined by the rule of mixture (see [Bao and Wang 1995])

$$E(z) = g(z)E_1 + [1 - g(z)]E_2, \tag{27}$$

where E_1 and E_2 are the Young's moduli of the bottom and top surfaces of the FGM plate, respectively ($z = \pm h/2$). The variation of the Young's modulus of a P-FGM plate in the thickness direction with different material parameters p is plotted in Figure 2, which indicates that the overall stiffness of the FGM plate increases as the parameter p decreases. It is seen from Figure 2 that the Young's modulus varies rapidly at the top surface ($z/h = -0.5$) of the plate, therefore it must be very carefully defined in finite element analysis when dividing the meshes near the top surface.
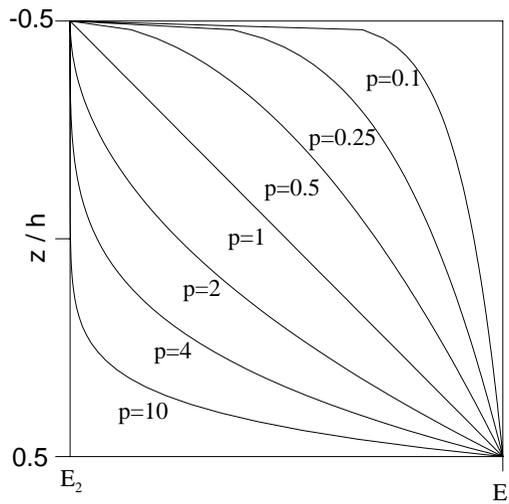

Figure 2. Variation of the Young's modulus of a P-FGM plate with differing material parameters p.

Substituting the gradation of the Young's modulus of P-FGM plates in (27) into the definition of coefficients in Equations (5), we obtain the coefficients of P-FGM plates:

$$A_{11} = \frac{h}{1-v^2}\Big(E_2 + (E_1 - E_2)\frac{1}{p+1}\Big),$$

$$B_{11} = \frac{h^2}{2(1-v^2)}(E_1 - E_2)\frac{p}{(p+1)(p+2)},$$

$$C_{11} = \frac{h^3}{12(1-v^2)}\Big(E_2 + (E_1 - E_2)\frac{3(p^2+p+2)}{(p+1)(p+2)(p+3)}\Big), \qquad (28)$$

$$Q_{11} = \frac{-ph}{2(p+2)}\frac{(E_1-E_2)}{(pE_2+E_1)},$$

$$S_{11} = \frac{h^3}{12(1-v^2)}\Big(E_2 + \frac{3(p^2+p+2)(E_1-E_2)}{(p+1)(p+2)(p+3)} - \frac{3p^2(E_1-E_2)^2}{(p+1)(p+2)^2(pE_2+E_1)}\Big).$$

4.2. *Material properties of S-FGM plates.* In the case of adding an FGM of a single power-law function to the multilayered composite, stress concentrations appear on one of the interfaces where the material is continuous but changes rapidly [Lee and Erdogan 1994; Bao and Wang 1995]. Therefore, we defined the volume fraction using two power-law functions to ensure smooth distribution of stresses among all the interfaces. The Young's modulus of the S-FGM plate is defined based on two power-law functions [Chung and Chi 2001]

$$g_1(z) = 1 - \frac{1}{2}\Big(\frac{h/2-z}{h/2}\Big)^p \quad \text{for } 0 \le z \le h/2, \qquad (29a)$$

$$g_2(z) = \frac{1}{2}\Big(\frac{h/2+z}{h/2}\Big)^p \qquad \text{for } -h/2 \le z \le 0. \qquad (29b)$$

By using the rule of mixture, the Young's modulus of the S-FGM plate can be calculated by

$$E(z) = g_1(z)E_1 + [1 - g_1(z)]E_2 \quad \text{for } 0 \le z \le h/2, \qquad (30a)$$
$$E(z) = g_2(z)E_1 + [1 - g_2(z)]E_2 \quad \text{for } -h/2 \le z \le 0. \qquad (30b)$$

The variation of the Young's modulus of a P-FGM plate in the thickness direction with different material parameters p is plotted in Figure 3 which shows that the material properties rapidly change near the top and bottom surfaces for $p \ll 1$ but vary rapidly near the middle surface for $p \gg 1$. Therefore, if the S-FGM plate is used as the undercoat in a laminated material, the material distribution with $p \gg 1$ is the better choice.
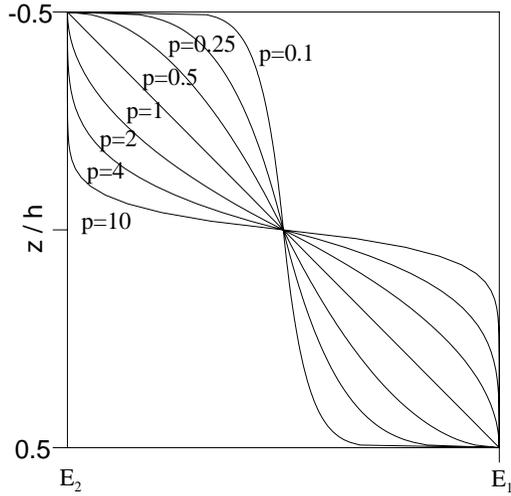
Figure 3. Variation of the Young's modulus of an S-FGM plate with differing material parameters p.

A similar approach to that used for P-FGM plates yields for the coefficients of S-GFM plates

$$A_{11} = \frac{h}{1-v^2}\left(\frac{E_1+E_2}{2}\right),$$

$$B_{11} = \frac{h^2}{8(1-v^2)}(E_1-E_2)\frac{p^2+3p}{(p+1)(p+2)},$$

$$C_{11} = \frac{h^3}{12(1-v^2)}\frac{E_1+E_2}{2}, \tag{31}$$

$$Q_{11} = \frac{-h(E_1-E_2)(p^2+3p)}{4(E_1+E_2)(p+1)(p+2)},$$

$$S_{11} = \frac{h^3}{8(1-v^2)}\left(\frac{E_1+E_2}{3} - \frac{(E_1-E_2)^2(p^2+3p)^2}{4(E_1+E_2)(p+1)^2(p+2)^2}\right).$$

4.3. *Physical meaning of the quantities A_{11}, B_{11}, and C_{11}.* For FGM plates with constant Poisson's ratio, the parameters A_{11}, B_{11}, and C_{11} are defined in (5a) as

$$(A_{11}, B_{11}, C_{11}) = \frac{1}{1-v^2}\int_{-h/2}^{h/2}\left(E(z), zE(z), z^2E(z)\right)dz$$

Therefore, it is clear that $(1-v^2)A_{11}$ equals the area under the $E(z)$ curve from $z = -h/2$ to $z = h/2$, referred to in Figure 4, as indicated in [Mushelishvili 1953]. Similarly, the parameters B_{11}, and C_{11} are related to the first and second moments of the area under the $E(z)$ curve from $z = -h/2$ to $z = h/2$ with
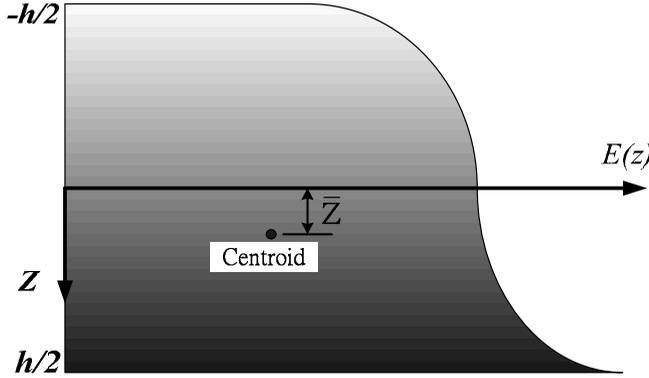
Figure 4. Distribution of the Young's modulus in the thickness direction of an FGM plate.

respect to the $z = 0$ axis. They are simplified as

$$(1 - v^2)A_{11} = \text{ the area under the } E(z) \text{ curve from } z = -h/2 \text{ to } z = h/2, \qquad (32a)$$

$$(1 - v^2)B_{11} = (1 - v^2)A_{11} \times \bar{z}, \qquad (32b)$$

$$(1 - v^2)C_{11} = \bar{I} + (1 - v^2)A_{11} \times \bar{z}^2, \qquad (32c)$$

where $\bar{z}$ is the distance from the centroid of the area $(1 - v^2)A_{11}$ to the axis $z = 0$, and $\bar{I}$ is the second moment of the area $(1 - v^2)A_{11}$ with respect to the axis passing through the centroid. It can be seen from Equation (32c) that the location of the centroid $\bar{z}$ can be expressed by the parameters A_{11} and B_{11} as

$$\bar{z} = \frac{B_{11}}{A_{11}}. \qquad (33)$$

From Equations (28) and (31), the quantity B_{11} is positive if the Young's moduli satisfy $E_1 > E_2$; in this case the location of the centroid $\bar{z}$ is also positive.

4.4. *Physical meaning of the parameters Q_{11} and S_{11}.* Because of the zero strains at the neutral surface, the neutral surface is located at $Q_{11} + z = 0$ according to (25e). Therefore, the physical meaning of the parameter Q_{11} is the negative of the location of the neutral surface of the FGM plates. Based on (15) where $Q_{11} = -B_{11}/A_{11}$ and (33) where $\bar{z} = B_{11}/A_{11}$, we obtain $Q_{11} + \bar{z} = 0$ which means that the axes of the neutral surface and the centroid of the area under the $E(z)$ curve coincide. Therefore, the neutral surface of the FGM plates for bending problems can be evaluated directly by determining the location of the centroid of the $E(z)$ curve, which is related to the quantity B_{11} in (33). Consequently, it is concluded that when the origin of the z-axis is located at the central axis of the area under the $E(z)$ curve parallel to the middle surface, the quantity $B_{11} = 0$.

The neutral surfaces versus the material parameter p with different ratios of Young's moduli are plotted in Figure 5 for P-FGM and S-FGM plates. The two halves of the figure indicate that the neutral axes move far away from the $z = 0$ axis as the parameter p increases for $E_1/E_2 > 1$ (with E_1 fixed). With the
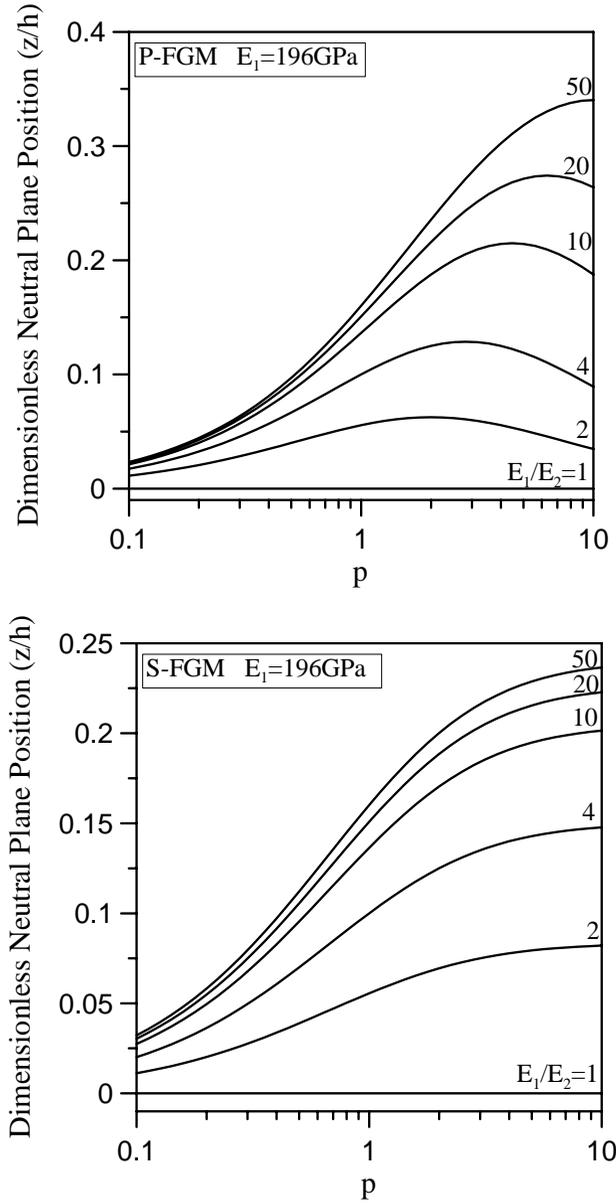
Figure 5. Locations of the neutral surfaces versus the material parameter p for $E_1 =$ 196 GPa and varying E_2. Top: P-FGM plate. Bottom: S-FGM plate.

same parameter p and Young's moduli E_1 and E_2, the locations of the neutral surfaces of the S-FGM plates are closer to the middle surfaces than those of the P-FGM plates.

It is also worthwhile to investigate the quantity S_{11}. With the aid of (15), (32c) and (33), the parameter S_{11} can be rewritten as

$$S_{11} = \frac{\bar{I}}{1 - \nu^2}, \tag{34}$$

where $\bar{I}$ is the second moment of the area $(1 - v^2)A_{11}$ with respect to the axis passing through the centroid. For homogeneous plates ($E_1 = E_2 = E$), the quantity S_{11} equals $Eh^3/12(1 - v^2)$ according to (28) and (31), and this is the bending stiffness of a homogeneous plate. By comparing the equilibrium equation of FGM plates in (16) with that of homogeneous plates, it is shown that parameter S_{11} is related to the bending stiffness of FGM plates. Therefore, the parameter S_{11} is here called the bending stiffness of FGM plates.
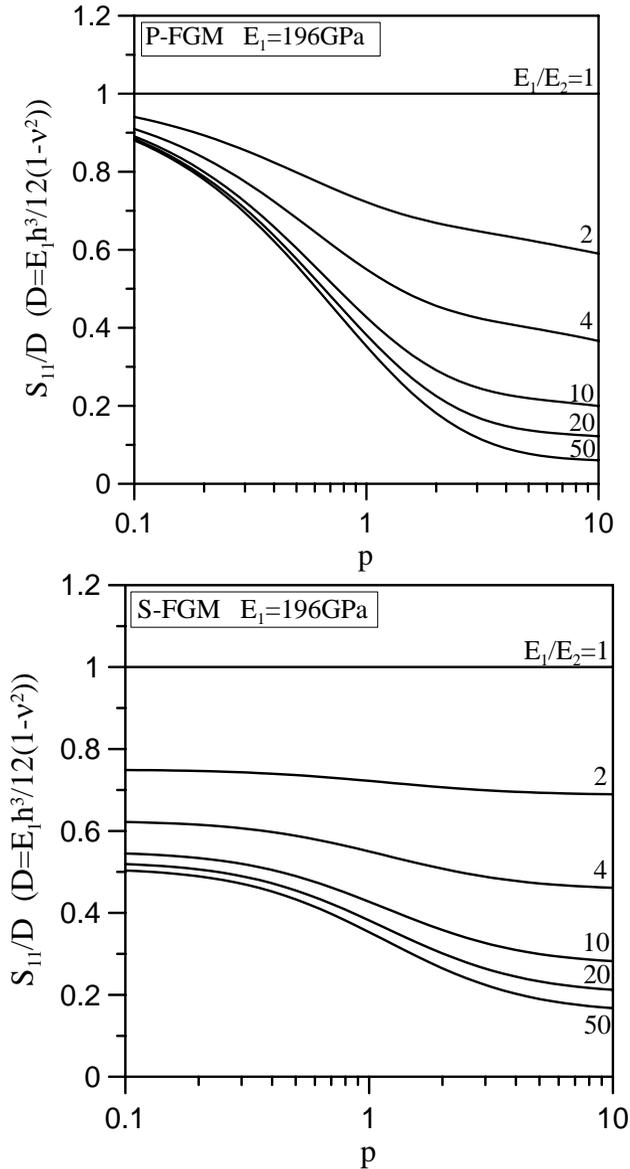
Figure 6. Bending stiffness versus material parameter p for $E_1 = 196\,\text{GPa}$ and varying E_2. Top: P-FGM plate. Bottom: S-FGM plate.

The ratios of S_{11} to the bending stiffness of homogeneous plates $Eh^3/12(1-v^2)$ are plotted in Figure 6 for P-FGM and S-FGM plates. The figure shows that $S_{11} = Eh^3/12(1-v^2)$ for a homogeneous plate in which $E_1 = E_2$. The bending stiffness of FGM plates S_{11} decreases with increase of p for $E_1/E_2 > 1$. However for P-FGM plates, the bending stiffnesses S_{11} are almost the same and close to that of the homogeneous plate for $p \ll 1$. It also can be seen that the bending stiffness S_{11} decreases when E_1/E_2 (E_1 fixed) increases for both S-FGM and P-FGM plates, because the overall stiffnesses of the plates decrease with the increase of E_1/E_2.

5. Numerical results

For the problem in Figure 1, if the aspect ratio a/b is large, the behavior of the plate will be similar to that of a beam. Therefore, consider a homogeneous plate in which $E_1 = E_2 = E$ and Poisson's ratio is $v = 0$ subjected to a uniform load q_0. If the aspect ratio a/b of the plate is large, the maximum deflection located at $x = a/2$ is approximated by $5q_0ba^4/384EI = 15q_0a^4/96Eh^3 = 0.15625q_0a^4/Eh^3$. This value will be compared with the solution to a homogeneous plate given in Equation (25a).

When $E_1 = E_2 = E$, and $v = 0$, Equations (28) and (31) become

$$(1-v^2)A_{11} = Eh, \qquad B_{11} = Q_{11} = 0, \qquad C_{11} = S_{11} = Eh^3/12(1-v^2).$$

As mentioned previously, the quantity $(1-v^2)A_{11}$ represents the area under the $E(z)$ curve from $z = -h/2$ to $z = h/2$ which is equal to Eh. The results of $Q_{11} = 0$ and $B_{11} = 0$ reveal that the location of the neutral surface is at the origin of the z-axis, and that the axes of the neutral surface and the centroid of the area under the $E(z)$ curve coincide, respectively. Moreover, the term $(1-v^2)C_{11}$, the second moment of the area under the $E(z)$ curve from $z = -h/2$ to $z = h/2$ with respect to $z = 0$ axis, is equal to the bending stiffness of FGM plates S_{11} times $(1-v^2)$.

The coefficients A_{1m} and A_{2m} in (24) are approximated by zero as the aspect ratio a/b becomes large. Then, the displacement of a homogeneous rectangular plate based on (25a) is simplified as $w(x, y) = \sum_m w_{mp}(y) \sin kx$. Hence, the maximum displacement of the homogeneous rectangular plate located at $y = 0$, $x = a/2$ is obtained as

$$w(x = a/2, y = 0) = \frac{48q_0a^4}{\pi^5 Eh^3} \sum_{m=1,3,5,...} \frac{1}{m^5} \sin \frac{m\pi}{2},$$

$$\approx 0.15625 \frac{q_0a^4}{Eh^3}. \tag{35}$$

The result of (35) derived from (25a) with $E_1 = E_2 = E$, $v = 0$ and large a/b is almost the same as the result from beam theory. The comparison of the deflections of a homogeneous plate and a beam is shown in Figure 7 for different aspect ratios. The figure shows that if the aspect ratio a/b is large, the deflections at the line $x = a/2$ based on the plate theory and beam formulation are almost the same for zero or nonzero Poisson's ratio. However if the aspect ratio a/b is small, the deflection at the center of the homogeneous plate will be identical to that of the beam theory only for Poisson's ratio $v = 0$.

Next, consider an FGM plate in which the boundary and load conditions are shown in Figure 1. Because of the symmetry about the x- and y-axes, only one quarter of the full plate in Figure 1 is under consideration when using the finite element program MARC. On the edge $y = 0$ of the one-quarter plate,
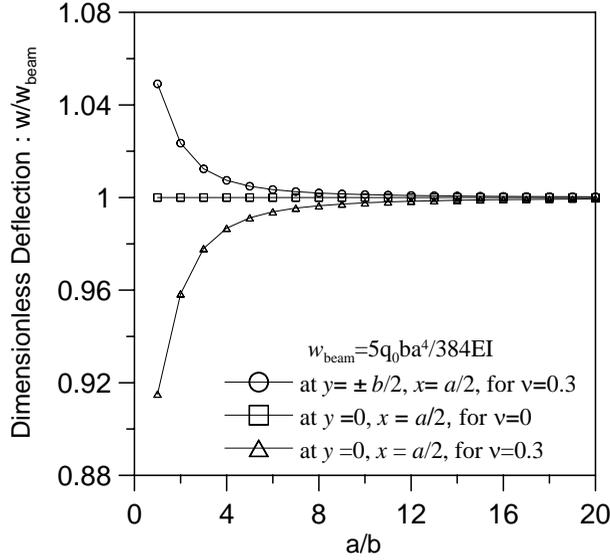
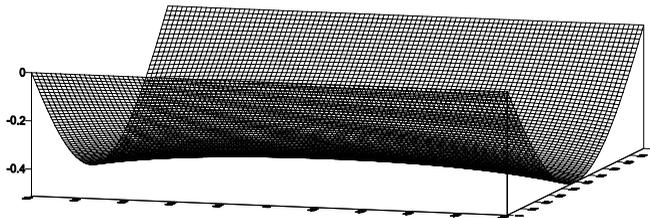**Figure 7.** Comparison of the deflections of a homogeneous plate and beam.

Figure 8. Deformation of an FGM plate at the neutral surface.

hinges are put at the neutral surface, while on the symmetric edges (that is, $y = 0$ and $x = a/2$), rollers are used such that displacements in z-direction are allowed. In the finite element mesh, because there is no stress singularity in the plate, solid eight-node elements are applied and 20×20 equally divided elements are used in the x- and y-directions. In order to simulate the variation of the material properties of the FGM plate, sixty layers in the thickness direction are used. Each layer has constant material properties, but the material properties differ from layer to layer. The material properties of all layers in the mesh are determined from the functions of volume fractions, according to the given E_1, E_2, v.

The dimensions of the FGM plate in Figure 1 are taken as $a = b = 100$ cm and $h = 2$ cm, so the width to thickness ratio is equal to 50. The Poisson's ratio of the FGM plate is assumed to be constant for the whole plate and is taken as $v = 0.3$. It is assumed that the Young's modulus at the bottom surface of the FGM plate E_1, is 196 GPa, while that at the top surface of the S-FGM plate E_2, varies with the ratio of E_1/E_2. The deflections and strains of the FGM plate for the material parameter $p = 2$ and the ratios of Young's modulus $E_1/E_2 = 1, 2, 4, 10, 20, 50$ are under investigation.

The deformed configuration of an FGM plate at the neutral surface is shown in Figure 8. The dimensionless deflections along the $x = a/2$ axis from $y = 0$ to $y = b/2$ and those along the $y = 0$ axis from
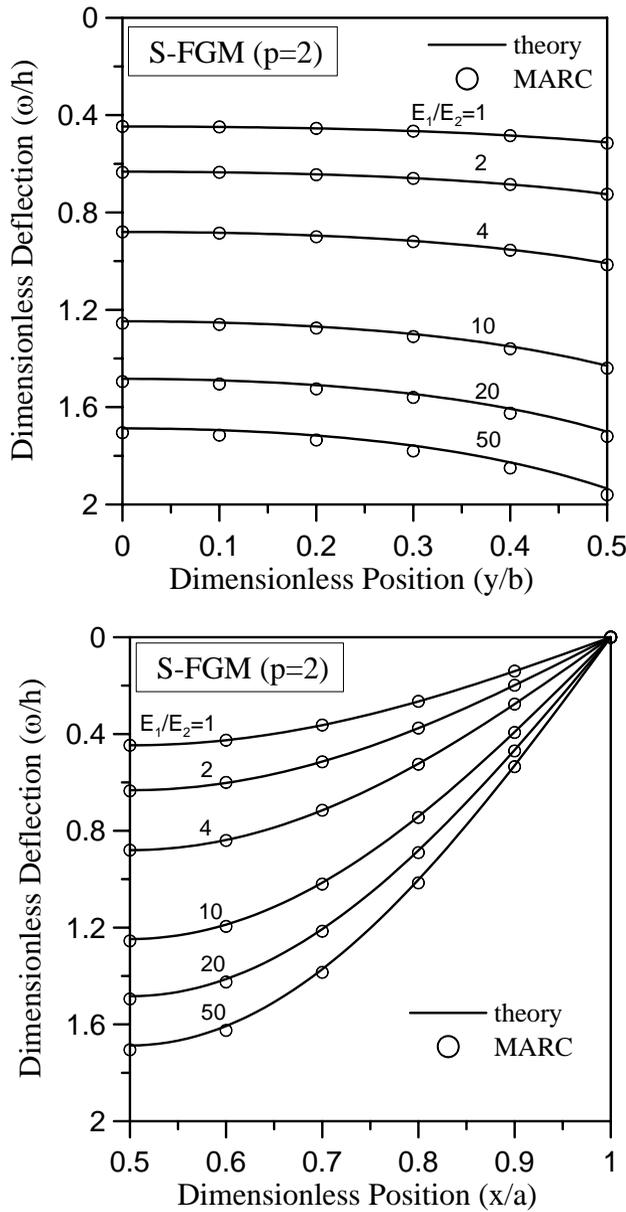
Figure 9. Deflection of an S-FGM plate. Top: from $y = 0$ to $y = b/2$ along the line $x = a/2$. Bottom: from $x = a/2$ to $x = a$ along the line $y = 0$.

$x = a/2$ to $x = a$ are plotted in Figure 9. Figures 8 and 9 reveal that the FGM plate exhibits saddle deformation which is the same as in homogeneous plates. The analytical and numerical results agree very well for small E_1/E_2 and are slightly different for large E_1/E_2. However, the error is less than 5%.

The dimensionless stresses σ_x/q_0 and σ_y/q_0 at the center of the plate along the thickness direction for $p = 2$ and different E_1/E_2 ratios are presented in Figure 10. These figures show that the stresses of the
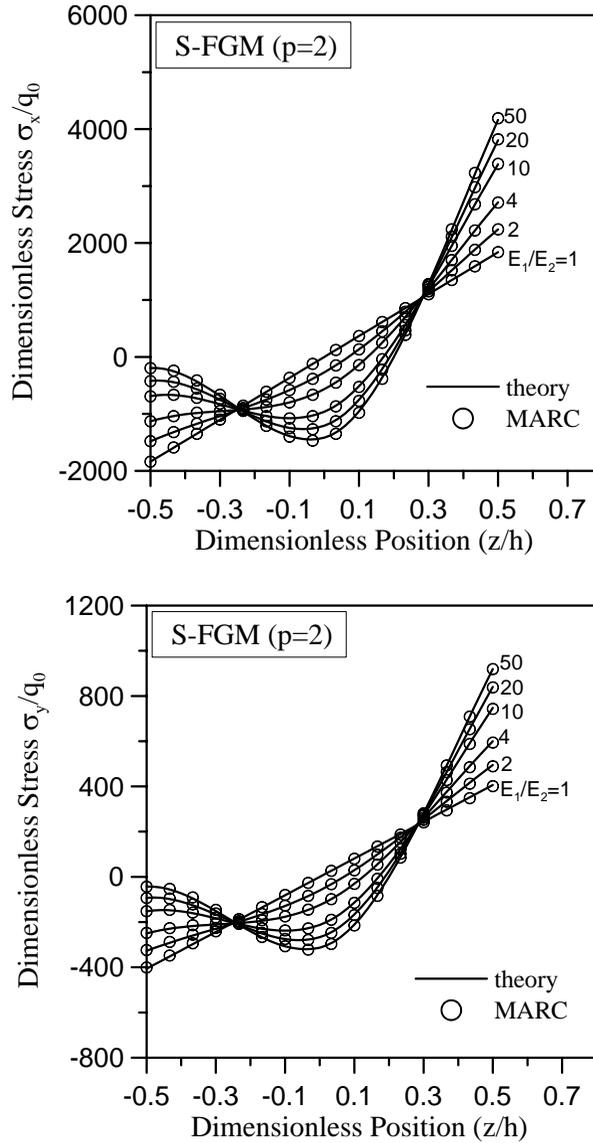
Figure 10. Distribution of stresses σ_x (top) and σ_y (bottom) at the center of an S-FGM plate along the thickness direction for different E_1/E_2 ratios.

S-FGM plate along the thickness direction are cubed. This is reasonable because the material parameter $p = 2$. For a homogeneous plate in which $E_1/E_2 = 1$, the magnitude of the tensile and compressive stresses are equal and located at the top and bottom surfaces. However, as the ratio of E_1/E_2 increases, the magnitudes of the tensile and compressive stresses are no longer equal. The maximum stress is tensile and is located at the bottom surface of the plate. However, the maximum compressive stress moves from the top surface to inside of the plate, and this phenomenon becomes clear for large E_1/E_2.
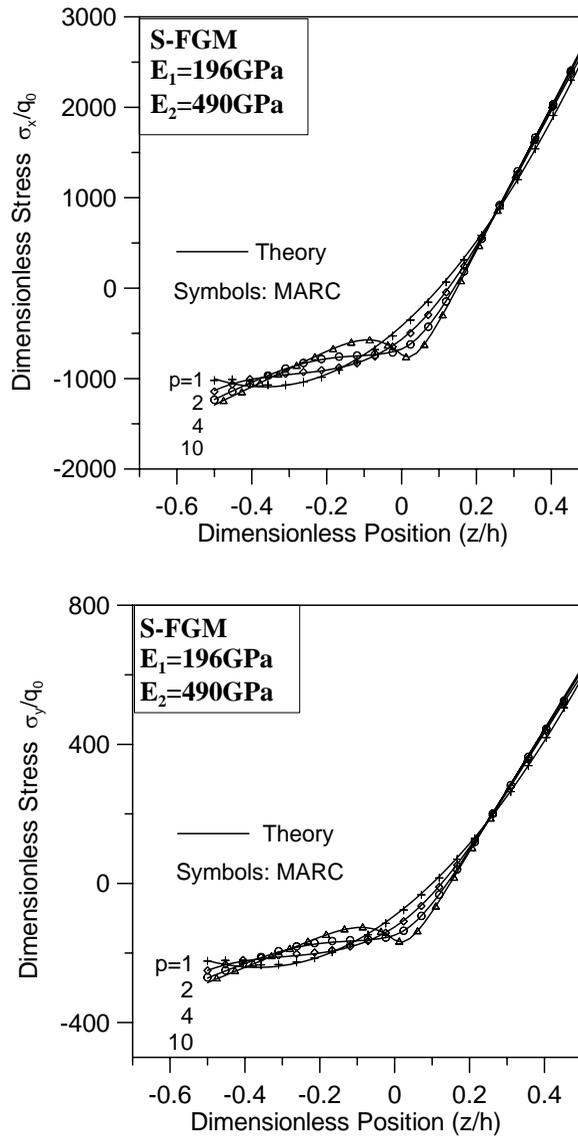
Figure 11. Distribution of stresses σ_x (top) and σ_y (bottom) at the center of an S-FGM plate along the thickness direction for differing material parameters $p \geq 1$.

Next we focus on a fixed value $E_1/E_2 = 4$, with changing material parameters $p = 1, 2, 4$, and 10, and $p = 1/2, 1/4$, and $1/10$. The dimensionless stresses σ_x/q_0 and σ_y/q_0 at the center of the FGM plates are plotted in Figure 11 for $p = 1, 2, 4$, and 10 and in Figure 12 for $p = 1/2, 1/4$, and $1/10$. It is clear from these four figures that the stress distributions differ little for different parameters p when E_1/E_2 is fixed. Specifically, the stresses at the top and bottom surfaces are almost the same for $p < 1$. This phenomenon occurs because the bending stiffness S_{11} for $E_1/E_2 = 4$ doesn't change very much for different values of p.
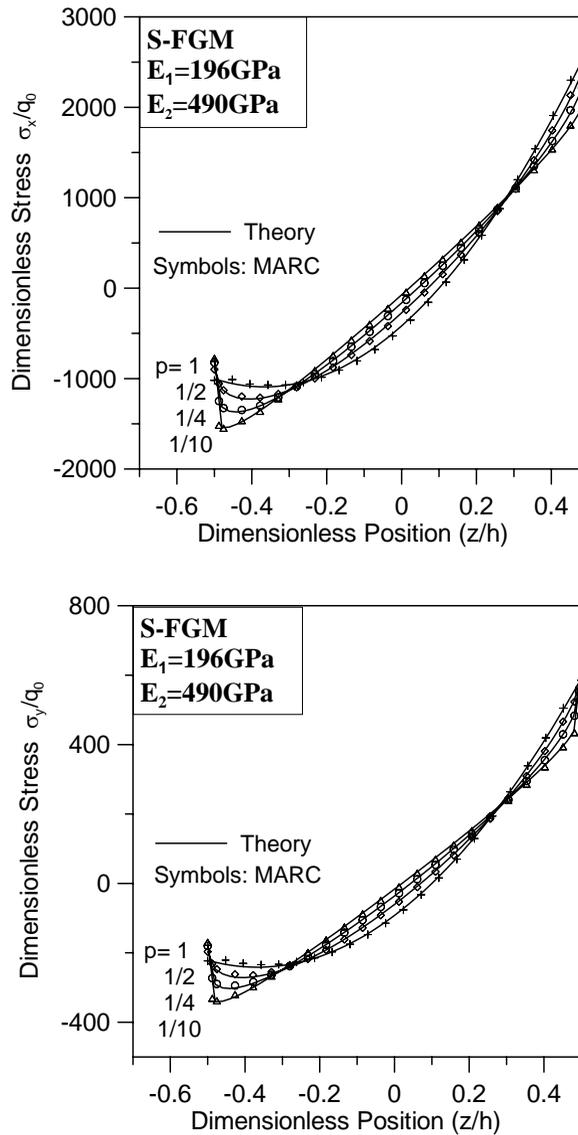
Figure 12. Distribution of stresses σ_x (top) and σ_y (bottom) at the center of an S-FGM plate along the thickness direction for differing material parameters $p < 1$.

So far, the results in this paper show that the analytical solution agrees very well with FEM simulation. However, the limitations and range of validity of the proposed model need to be investigated. Therefore, further considerations will focus on how thick the FGM plate is, or how steep the material gradient can be for the theoretical solution to fail.

The theoretical solutions in this paper are based on the assumption that the thickness of a moderately thick FGM plate is in the range $1/20 \sim 1/100$ of its span, and thus transverse shear deformations can be negligible. To examine this assumption, we fix the ratio $E_1/E_2 = 10$ but take the thickness of the
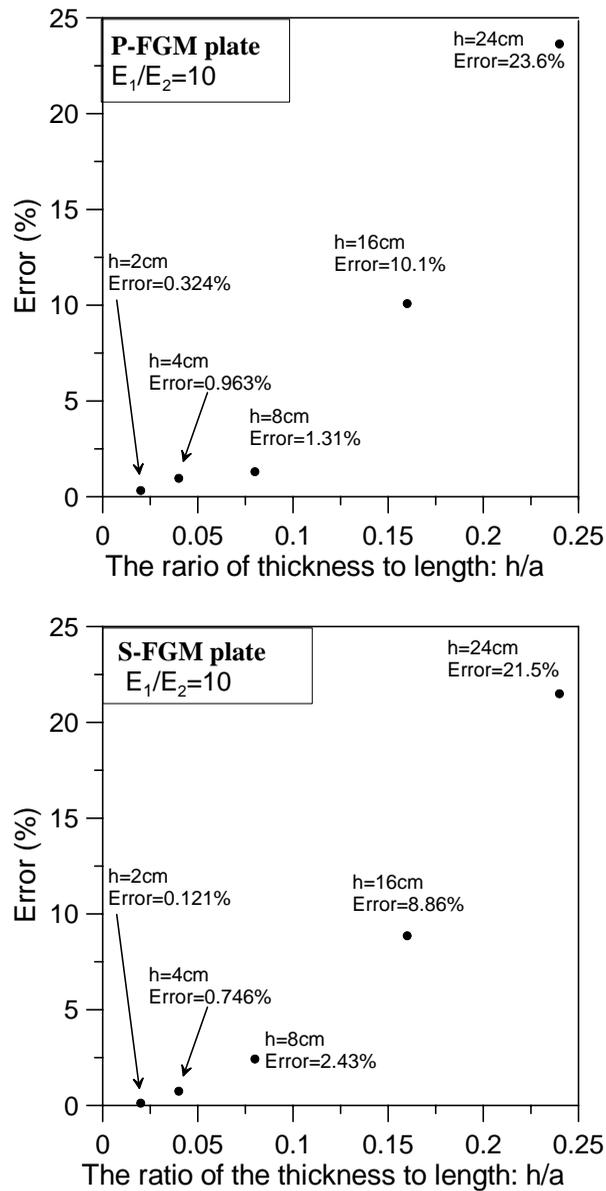
Figure 13. Error in maximum deflection versus thickness-to-length ratio h/a (fixed a). Top: P-FGM plate; bottom: S-FGM plates. In both cases $E_1/E_2 = 10$.

plate $h = 2\,\text{cm}$, $4\,\text{cm}$, $8\,\text{cm}$, $16\,\text{cm}$, or $24\,\text{cm}$, and the corresponding ratios of thickness to length $h/a = 0.02, 0.04, 0.08, 0.16, 0.24$. The maximum deflections located at the center of the plate are evaluated by theoretical equation and FEM simulation. The errors, which are the differences between theoretical and numerical results divided by the theoretical results, are plotted in Figure 13 for P-FGM and S-FGM plates for various ratios h/a. These figures indicate that for moderately thick FGM plates with thickness less than 0.1 of the span, the error is less than 5%. This means that for an FGM plate with thickness
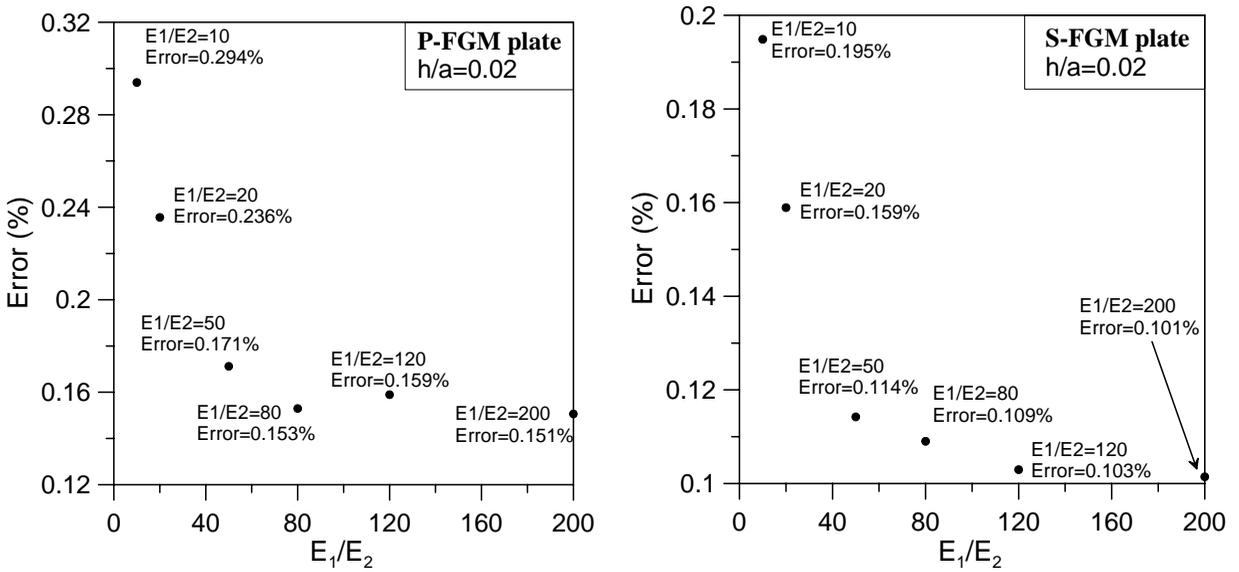
Figure 14. Error of maximum deflection of P-FGM plates versus ratio E_1/E_2 between Young's moduli. Top: P-FGM plate; bottom: S-FGM plates. In both cases $h/a = 0.02$.

less than 0.1 of its span, the classical theory of plates will give good results, as indicated in [Shames and Dym 1985] for homogeneous plates.

To investigate the effect of the steepness of the material gradient on the FGM plates, the ratio of thickness to length is fixed at 0.02 (that is, $h/a = 0.02$), but the ratios of Young's moduli are taken as $E_1/E_2 = 1, 10, 20, 50, 80, 120$, and 200. The errors in maximum deflections versus the ratios E_1/E_2, plotted in Figure 14 for P-FGM and S-FGM plates, are all in the range 0.1% to 0.5%. Therefore, the linear assumption for the displacement field is still accurate for FGMs with steep material gradients.

6. Conclusions

We applied a Fourier series expansion to the analysis of FGM plates with two opposite edges simply supported and the other two edges free, subjected to uniform load. The results lead to these conclusions:

(1) The analytical solution obtained agrees very well with the finite element solution. The deformed configuration of the FGM plates is a saddle deformation, which is the same as that of a homogeneous plate. The maximum tensile stresses are located at the bottom of the FGM plates. However, the maximum compressive stresses move to the inside of the FGM plates, especially for larger E_1/E_2.

(2) In general, the bending and in-plane problems in FGM plates are coupled. But if the material properties of the FGM plate are such that the Young's modulus varies along the thickness direction but the Poisson's ratio is constant for the whole FGM plate, as in the problem solved in this paper, then the governing equations for the bending and in-plane problem become uncoupled.

(3) The parameters of A_{11}, B_{11}, C_{11}, Q_{11}, and S_{11} defined in this paper have physical meaning. The quantity $(1 - \nu^2)A_{11}$ represents the area under the $E(z)$ curve from $z = -h/2$ to $z = h/2$. The

parameters B_{11} and C_{11} are related to the first and second moment of the area under the $E(z)$ curve from $z = -h/2$ to $z = h/2$ with respect to the $z = 0$ axis. The ratio of B_{11}/A_{11} is equal to the centroid location $\bar{z}$, of the area under the $E(z)$ curve. The parameter $Q_{11} = -B_{11}/A_{11} = -\bar{z}$ represents the location of the centroid of the area under the $E(z)$ curve. The parameter S_{11} is called here the bending stiffness of FGM plates.

References

[Bao and Wang 1995] G. Bao and L. Wang, "Multiple cracking in functionally graded ceramic/metal coatings", *Int. J. Solids Struct.* **32**:19 (1995), 2853–2871.

[Cai and Bao 1998] H. Cai and G. Bao, "Crack bridging in functionally graded coatings", *Int. J. Solids Struct.* **35**:7–8 (1998), 701–717.

[Chi and Chung 2002] S. H. Chi and Y. L. Chung, "Cracking in sigmoid functionally graded coating", *J. Mech.* **18** (2002), 41–53.

[Chi and Chung 2003] S. H. Chi and Y. L. Chung, "Cracking in coating-substrate composites of multi-layered and sigmoid FGM coatings", *Eng. Fract. Mech.* **70**:10 (2003), 1227–1243.

[Chi and Chung 2006a] S. H. Chi and Y. L. Chung, "Mechanical behavior of functionally graded material plates under transverse load, I: Analysis", *Int. J. Solids Struct.* **43**:13 (2006), 3657–3674.

[Chi and Chung 2006b] S. H. Chi and Y. L. Chung, "Mechanical behavior of functionally graded material plates under transverse load, II: Numerical results", *Int. J. Solids Struct.* **43**:13 (2006), 3675–3691.

[Chung and Chi 2001] Y. L. Chung and S. H. Chi, "The residual stress of functionally graded materials", *J. Chin. Inst. Civil. Hydraul. Eng.* **13** (2001), 1–9.

[Delale and Erdogan 1983] F. Delale and F. Erdogan, "The crack problem for a nonhomogeneous plane", *J. Appl. Mech.* (*ASME*) **50** (1983), 609–614.

[Erdogan and Chen 1998] F. Erdogan and Y. F. Chen, "Interfacial cracking of FGM/metal bonds", pp. 29–37 in *Ceramic coating*, edited by K. Kokini, 1998.

[Erdogan and Wu 1996] F. Erdogan and B. H. Wu, "Crack problems in FGM layers under thermal stresses", *J. Therm. Stresses* **19** (1996), 237–265.

[Feldman and Aboudi 1997] E. Feldman and J. Aboudi, "Buckling analysis of functionally graded plates subjected to uniaxial loading", *Compos. Struct.* **38**:1–4 (1997), 29–36.

[Ferreira et al. 2005] A. J. M. Ferreira, R. C. Batra, C. M. C. Roque, L. F. Qian, and P. A. L. S. Martins, "Static analysis of functionally graded plates using third-order shear deformation theory and a meshless method", *Compos. Struct.* **69**:4 (2005), 449–457.

[Gu and Asaro 1997] P. Gu and R. J. Asaro, "Crack deflection in functionally graded materials", *Int. J. Solids Struct.* **34**:24 (1997), 3085–3098.

[He et al. 2001] X. Q. He, T. Y. Ng, S. Sivashanker, and K. M. Liew, "Active control of FGM plates with integrated piezoelectric sensors and actuators", *Int. J. Solids Struct.* **38**:9 (2001), 1641–1655.

[Jin and Batra 1996] Z. H. Jin and R. C. Batra, "Stress intensity relaxation at the tip of an edge crack in a functionally graded material subjected to a thermal shock", *J. Therm. Stresses* **19** (1996), 317–339.

[Jin and Noda 1994] Z. H. Jin and N. Noda, "Crack tip singular fields in nonhomogeneous materials", *J. Appl. Mech.* (*ASME*) **61** (1994), 738–740.

[Jin and Paulino 2001] Z. H. Jin and G. H. Paulino, "Transient thermal stress analysis of an edge crack in a functionally graded material", *Int. J. Fract.* **107**:1 (2001), 73–98.

[Kesler et al. 1997] O. Kesler, M. Finot, S. Suresh, and S. Sampath, "Determination of processing-induced stresses and properties of layered and gradedcoatings: experimental method and results for plasma-sprayed Ni-Al$_2$O$_3$", *Acta Mater.* **45**:8 (1997), 3123–3134.

[Kwon and Crimp 1997] P. Kwon and M. Crimp, "Automating the design process and powder processing of functionally gradient materials", pp. 73–88 in *Composites and functionally graded materials: 1997 ASME International Mechanical Engineering Congress and Exposition*, edited by T. S. Srivatsan et al., ASME MD **80**, AMSE, New York, 1997.

[Lee and Erdogan 1994] Y. D. Lee and F. Erdogan, "Residual/thermal stress in FGM and laminated thermal barrier coatings", *Int. J. Fract.* **69**:2 (1994), 145–165.

[Ma and Wang 2004] L. S. Ma and T. J. Wang, "Relationships between axisymmetric bending and buckling solutions of FGM circular plates based on third-order plate theory and classical plate theory", *Int. J. Solids Struct.* **41**:1 (2004), 85–101.

[Mushelishvili 1953] N. I. Mushelishvili, *Some basic problems of the mathematical theory of elasticity*, Noordhoff, Groningen, 1953.

[Nowinski and Turski 1953] J. Nowinski and S. Turski, "On the theory of elasticity of isotropic non-homogeneous bodies", *Arch. Mech.* **5** (1953), 67–83. In Polish.

[Obata and Noda 1996] Y. Obata and N. Noda, "Optimum material design for functionally gradient material plate", *Arch. Appl. Mech.* **66**:8 (1996), 581–589.

[Praveen and Reddy 1998] G. N. Praveen and J. N. Reddy, "Nonlinear transient thermoelastic analysis of functionally graded ceramic-metal plates", *Int. J. Solids Struct.* **35**:33 (1998), 4457–4476.

[Shames and Dym 1985] I. H. Shames and C. L. Dym, *Energy and finite element methods in structural mechanics*, McGraw-Hill, New York, 1985.

[Sofiyev 2004] A. H. Sofiyev, "The stability of functionally graded truncated conical shells subjected to aperiodic impulsive loading", *Int. J. Solids Struct.* **41**:13 (2004), 3411–3424.

[Sokolowski 1958] M. Sokolowski, "The bending of transversally non-homogeneous plates of moderate thickness", *Arch. Mech.* **10** (1958), 315–328.

[Suresh and Mortensen 1998] S. Suresh and A. Mortensen, *Fundamentals of functionally graded materials*, Cambridge University Press, 1998.

[Tauchert 1986] T. R. Tauchert, "Thermal stresses in plates: static problems", pp. 23–141 in *Thermal stresses, I*, edited by R. B. Hetnarski, Elsevier, Amsterdam, 1986.

[Vel and Batra 2002] S. S. Vel and R. C. Batra, "Exact solution for thermoelastic deformations of functionally graded thick rectangular plates", *AIAA J.* **40**:7 (2002), 1421–1433.

[Vel and Batra 2003] S. S. Vel and R. C. Batra, "Three-dimensional analysis of transient thermal stresses in functionally graded plates", *Int. J. Solids Struct.* **40**:25 (2003), 7181–7196.

[Woo and Meguid 2001] J. Woo and S. A. Meguid, "Nonlinear analysis of functionally graded plates and shallow shells", *Int. J. Solids Struct.* **38**:42–43 (2001), 7409–7421.

[Wu et al. 2005] L. Wu, Z. Jiang, and J. Liu, "Thermoelastic stability of functionally graded cylindrical shells", *Compos. Struct.* **70**:1 (2005), 60–68.

YEN-LING CHUNG: chungyl@mail.ntust.edu.tw
Department of Construction Engineering, National Taiwan University of Science and Technology, P. O. Box 90-130, Taipei 10672, Taiwan

WEI-TING CHEN: *Department of Construction Engineering, National Taiwan University of Science and Technology, P. O. Box 90-130, Taipei 10672, Taiwan*